Enhancement of the Photoelectrochemical Performance of CuWO 4 Thin Films for Solar Water Splitting by Plasmonic Nanoparticle Functionalization

ARTICLE *in* THE JOURNAL OF PHYSICAL CHEMISTRY C · DECEMBER 2014

Impact Factor: 4.77 · DOI: 10.1021/jp506349t

5 AUTHORS, INCLUDING:

Marco Valenti
Delft University of Technology
7 PUBLICATIONS **7** CITATIONS
SEE PROFILE

D. Dolat
Delft University of Technology
16 PUBLICATIONS **162** CITATIONS
SEE PROFILE

Wilson Smith
Delft University of Technology
33 PUBLICATIONS **601** CITATIONS
SEE PROFILE

THE JOURNAL OF PHYSICAL CHEMISTRY C

Article

pubs.acs.org/JPCC

Enhancement of the Photoelectrochemical Performance of $CuWO_4$ Thin Films for Solar Water Splitting by Plasmonic Nanoparticle Functionalization

M. Valenti,[†] D. Dolat,[†] G. Biskos,[†,‡,§,∥] A. Schmidt-Ott,[†] and W. A. Smith*[,†]

[†]Materials for Energy Conversion and Storage (MECS), Department of Chemical Engineering, Faculty of Applied Sciences, Delft University of Technology, Julianalaan 136, Delft 2628-BL, The Netherlands

[‡]Faculty of Civil Engineering and Geosciences, Delft University of Technology, Delft 2628-CN, The Netherlands

[§]Department of Environment, University of the Aegean, Mytilene 81100, Greece

[∥]Energy Environment and Water Research Center, The Cyprus Institute, Nicosia 1645, Cyprus

Supporting Information

ABSTRACT: The effect of plasmonic nanoparticles (NPs) on the photoelectrochemical water splitting performance of $CuWO_4$ is studied here for the first time. $CuWO_4$ thin films were functionalized with well-defined Au NPs in two composite configurations: with the NPs (I) at the $CuWO_4$–electrolyte interface and (II) at the $CuWO_4$ back contact. In both cases, the incident photon to current conversion efficiency of the film was increased (~6-fold and ~1.2-fold for configurations I and II (at λ = 390 nm), respectively). Two important advantages of placing the NPs on the $CuWO_4$–electrolyte interface are identified: (1) Au NPs, coated with a 2 nm TiO_2 layer, are found to significantly enhance the surface catalysis of the film, decreasing the surface charge recombination from ~60% to ~10%, and (2) the NP's near-field can promote additional charge carriers within the space charge layer region, where they undergo field-assisted transport, essentially avoiding recombination. Our study shows that Au NPs, coated with a 2 nm TiO_2 layer, can significantly mitigate the catalytic and optical photoelectrochemical (PEC) limitations of $CuWO_4$. An increase from 0.03 to 0.1 mA cm^{-2} in the water-splitting photocurrent was measured for a 200 nm film under simulated solar irradiation at 1.23 V vs RHE.

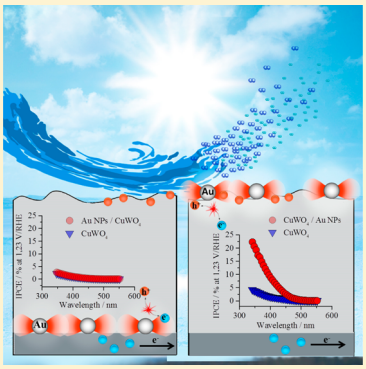

1. INTRODUCTION

Harvesting and storing solar energy in chemical bonds is an ideal alternative to fossil fuels and an answer to the continuously growing need for clean, renewable, and sustainable energy. One of the most promising ways to convert solar energy directly into fuel is by photoelectrochemical (PEC) water splitting, which can be achieved by light-absorbing semiconductors driving the oxygen and hydrogen evolution reactions.

Metal oxides are promising materials for solar water-splitting applications due to their low cost and high stability in aqueous environments. Nevertheless, their optoelectronic and catalytic properties result in a limited overall reaction efficiency, which needs further improvement. A large number of metal oxides have been investigated as photoelectrodes for water oxidation and reduction reactions. The most studied metal oxides (i.e., TiO_2, WO_3, Fe_2O_3) suffer from poor solar to hydrogen (STH) conversion efficiencies due to their large band gap energies (e.g., 3.2 eV for TiO_2[1] and 2.8 eV for WO_3[2]) and extremely short charge carrier diffusion lengths (e.g., 2 nm in Fe_2O_3).[3] $CuWO_4$ and $BiVO_4$ have recently attracted attention due to their relatively smaller band gap energies (2.4 eV for $BiVO_4$ and 2.25 eV for $CuWO_4$) and improved charge mobility characteristics.

In particular, polycrystalline $CuWO_4$ is a promising photoanode material.[4,5] The band gap of $CuWO_4$ is close to ideal for PEC water splitting (i.e., between 2.0 and 2.25 eV),[6] corresponding to a theoretical STH efficiency of ~13% (assuming 100% Faradaic efficiency) achieved at photocurrent density of 10.7 mA cm^{-2}.[7] Despite that, the PEC performance of $CuWO_4$ is significantly hindered by its low light absorption coefficient (e.g., ~10^3 cm^{-1} for $CuWO_4$[4] and ~10^5 cm^{-1} for Fe_2O_3[8] at λ = 500 nm) and high bulk charge transfer resistance,[5,9−11] which results in lower than theoretically possible photocurrent densities for this material.

Functionalizing semiconductors with plasmonic nanoparticles (NPs) can help mitigate some of their PEC water splitting limitations (e.g., low light absorption and charge carrier diffusion).[12] Under visible-light irradiation, valence electrons in noble metal NPs undergo a collective oscillatory motion. This phenomenon, called surface plasmon resonance (SPR), can enhance the PEC performance of nearby semiconductors by several mechanisms including (1) plasmon resonance energy transfer (PRET),[12] (2) hot electron injection,[13] and/or (3)

Received: June 26, 2014
Revised: December 18, 2014
Published: December 18, 2014

DOI: 10.1021/jp506349t
J. Phys. Chem. C 2015, 119, 2096−2104

light scattering, which will be described in subsections 1.1, 1.2, and 1.3, respectively.

Plasmon-enhanced solar water splitting has been studied for different systems including Fe_2O_3,[14] TiO_2,[12,15] and $BiVO_4$,[16] but so far it has not been used on $CuWO_4$. Thimsen et al.[14] functionalized iron oxide (Fe_2O_3) platelets with Au NPs (~45 nm in diameter). Due to the small overlap of the light absorption spectra of the NPs and the semiconductor used in that study, only a small increase in the normalized incident photon to current conversion efficiency (~25%) was observed. It should be noted that the relative enhancement reported in that study was measured only at the wavelengths where the absorption spectra of the NPs and semiconductor overlapped. On the other hand, Ingram et al.[12] reported a significant improvement in the solar hydrogen formation of a N-doped TiO_2 film (~750 nm thick) after functionalization with Au NPs or Ag nanocubes. The explanation provided by the authors is that the NP functionalization increased the surface charge carrier concentration in the semiconductor, which is particularly important for semiconductors, like TiO_2, that suffer from high bulk charge transfer resistance.

In either case, the above-mentioned studies highlight (1) the importance of tuning the NP plasmon resonance through their size and shape control (according to Mie theory) so as to match the absorption spectra of the applied semiconductor and (2) that NP functionalization can be an adequate way to improve significantly the semiconductors' performance and therefore mitigate their main inherent limitations.

In this work we investigate the possibilities of mitigating the inherent limitations of $CuWO_4$ (low absorption coefficient and large charge transfer resistance) by functionalizing relatively thin (200 nm) $CuWO_4$ films with plasmonic NPs. We deposit tailored 35 nm Au NPs, synthesized with a novel gas-phase technique, on $CuWO_4$ films in order to enhance their light absorption in the region near the band gap edge (i.e., ~ 540 nm) where the semiconductor exhibits its lowest absorption and PEC performance. According to Mie theory, spherical 35 nm Au NPs exhibit resonance frequencies around 540 nm.

Different mechanisms for plasmon-enhanced solar water splitting are briefly described below as a background for interpreting the results obtained in this study and to determine the most likely mechanisms for the enhancement of $CuWO_4$ water-splitting performance.

1.1. Plasmon Resonance Energy Transfer (PRET). An important characteristic of SPR is the enhancement of the incident electric field around the NP (NP near-field). When the NP is in contact or within a few nanometers from the semiconductor, its near-field penetrates the semiconductor as illustrated in Figure 1. In this region, the NP near-field acts as a light concentrator, locally enhancing the electron–hole generation rate in the semiconductor. This plasmon resonance energy transfer (PRET) enhancement mechanism is effective only for NPs with resonance frequencies that correspond to energies within the semiconductor's band gap.[14,17,18]

When the plasmonic NPs are placed on the semiconductor–electrolyte interface, the enhancement in the electron–hole formation rate will take place at the space charge layer (SCL). As a consequence, all the additional charge carriers formed due to the PRET will undergo field-assisted transport and contribute to the photocurrent. Hence, when the thickness of the film is larger than the SCL width, the PRET contribution is expected to be more significant when the NPs are placed near

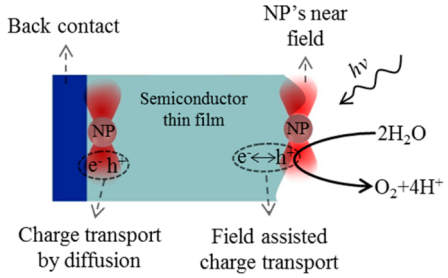

Figure 1. Illustration of the PRET enhancement mechanism induced by NPs placed on the semiconductor–electrolyte interface (right-hand side) and on the $CuWO_4$ back contact (left-hand side).

the semiconductor–electrolyte interface than at the semiconductor back contact.

1.2. Light Scattering. When the SPR decays, light is either scattered or absorbed.[19] According to Mie theory, if Au NPs are larger than 60 nm their scattering cross section in an aqueous environment becomes significant (>800 nm^2 at a wavelength of 540 nm). When the NPs are placed at an interface between two different materials, more light is scattered into the material with a larger refractive index (RI).[20] Since most metal oxides have a larger RI than water, plasmonic NPs placed at the semiconductor–electrolyte interface can reduce the amount of light that is reflected off the surface, by scattering the incident light into the semiconductor (Figure 2A). If the RI of the

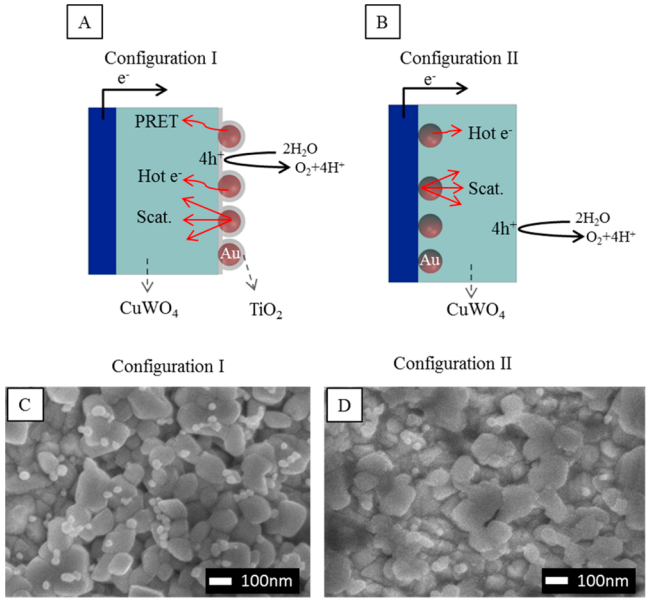

Figure 2. (A) and (B) Illustration of two $CuWO_4$–NP composite configurations in contact with an electrolyte. In Configuration I, TiO_2-coated Au NPs are placed at the $CuWO_4$–electrolyte interface, whereas in Configuration II the Au NPs are at the back contact. The most relevant optical effects are illustrated in each configuration. Scat. = scattering. (C) and (D) Corresponding SEM top-view images for the fabricated composite configurations.

semiconductor is also larger than the RI of the conducting back contact material, NPs placed at this interface will again have a preferential scattering toward the semiconductor (Figure 2B). Besides this antireflection effect, scattering of light at the surface of the semiconductor can also increase the light's path length through the semiconductor, which is critical for thin

DOI: 10.1021/jp506349t
J. Phys. Chem. C 2015, 119, 2096–2104

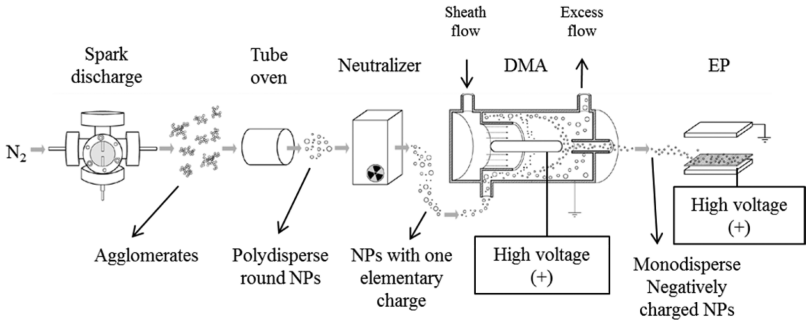

Figure 3. Schematic illustration of the synthesis and deposition of the monodisperse (35 nm in diameter) spherical Au NPs.

films with indirect band gap energies and small absorption coefficients.

Overall, the light-scattering mechanism induced by the NPs can increase the incident photon to current conversion efficiency (IPCE) of the semiconductor by increasing the light absorption. However, unlike the previously described enhancement mechanism (PRET), scattering does not enhance the *absorbed* photon to current conversion efficiency (APCE). Hence, APCE is a key measurement technique to distinguish between these two enhancement mechanisms.

1.3. Direct Hot Electron Injection. Small noble metal NPs having a large cross section of absorption can transfer the energy of resonating photons to the surrounding medium by the formation of charge carriers,[21] namely, hot electrons and holes. If the energy of the hot electron/hole is larger than the energy barrier at the NP−semiconductor interface, they can be transferred to the semiconductor's conduction/valence band and take part in the corresponding water-splitting half reactions.[13]

An important feature of this mechanism is that it can take place outside the semiconductor band gap energy, expanding the spectrum of usable light to longer wavelengths. This feature is used in this work to distinguish the hot electron injection mechanism from the aforementioned mechanisms (i.e., PRET and light scattering).

2. EXPERIMENTAL SECTION

2.1. Spray Deposition of $CuWO_4$ Thin-Film Photoanodes. Thin films (200 nm) of $CuWO_4$ were deposited on fluorine-doped tin oxide (FTO) substrate (TEC-15, Hartford Glass Co.) using an easy to scale-up spray pyrolysis technique. Prior to the $CuWO_4$ deposition, the substrate was cleaned by subsequent ultrasonication in triton, acetone, and isopropanol solution for ca. 20 min, dried under compressed N_2 flow, and slowly heated to 300 °C. The precursor solution was prepared by mixing preprepared 0.2 M aqueous solutions of copper sulfate pentahydrate ($CuSO_4{\cdot}5H_2O$, 99%, Acros Organics) and sodium tungstate dihydrate ($Na_2WO_4{\cdot}2H_2O$, 99%, Merck KGaA) and diluting with Milli-Q water to a concentration of 0.005 M. The pH of the final solution was adjusted to 10.5 by adding an appropriate amount of ammonia−water (NH_4OH, 25%, Sigma-Aldrich). The spray deposition was carried out using an automated spray setup with Quickmist air atomizing spray nozzle driven by an overpressure of 0.06 MPa of nitrogen gas. The distance between nozzle and substrate was fixed at 30 cm. Each spray cycle (5 cycles for 200 nm film) consisted of 2 s of spray time and 58 s of delay time to allow solvent evaporation. The resulting thin films were subsequently annealed for 4 h under air flow (20 mL min^{-1}) in a tube furnace at 500 °C, to ensure that the $CuWO_4$ is fully crystalline. The mean thickness (±20%) of the films was determined using a profilometer (DekTak 3).

2.2. NP Synthesis. Au NPs were synthesized in the gas phase with a spark discharge particle generator.[22] In brief, sparks between two gold electrodes are repeatedly formed with a frequency of 300 Hz using a power supply coupled with a capacitor. Gold vapors produced during every spark are carried away and cooled in a N_2 gas flow (2 L min^{-1}). As a result, the gold vapors condense into clusters that grow to NPs and agglomerate. The agglomerated NPs are sintered into spherical NPs by heating the aerosol flow in a tube furnace (~900 °C). The spherical NPs are then brought to the Boltzmann equilibrium charge distribution[23] by passing them through a neutralizer. The charged NPs leaving the neutralizer are mostly singly charged (e.g., > 95% for 50 nm NPs). A custom-made differential mobility analyzer (DMA[24]) downstream from the neutralizer is then used to separate the NPs according to their electrical mobility, which for singly charged NPs corresponds to the NP size (see eqs S1 and S2 in the Supporting Information).

By adjusting the operating conditions (i.e., voltage and flows) of the DMA, we selected 35 nm Au NPs, which were then deposited on the $CuWO_4$ film (or bare FTO substrate) for 15 min, using an electrostatic precipitator (EP). An illustration of the whole process of Au NP synthesis, size selection, and deposition is shown in Figure 3.

The size-selected Au NPs were also collected on a carbon polymer microgrid (supported on a copper grid) for characterization by transmission electron microscopy (TEM). From the TEM micrographs the NPs' cross-sectional areas were measured with the software *imagej* (Research Services Branch, National Institutes of Health), regardless of their shape. The effective NPs' diameters were then calculated from their corresponding areas by assuming spherical NPs (diameter = $2{\cdot}(\text{Area}/\pi)^{1/2}$). With this method, the sizes of 276 NPs were used to calculate the mean size of the synthesized NPs.

2.3. TiO_2 Deposition. A thin titanium dioxide layer with a thickness of 2.3 nm (determined by Ellipsometry) was deposited on top of the $CuWO_4$/Au NP films by atomic layer deposition (ALD) using tetrakis-dimethylamino titanium (TDMAT) and H_2O as precursors. ALD is a variant of chemical vapor deposition (CVD) used for growing ultrathin and high quality films.[25] The ALD equipment used for TiO_2 deposition is described in detail elsewhere.[26] The pulse sequences for depositions were 30 s for purge, 5 s for TDMAT precursor, 30 s for purge, and finally 10 ms for the H_2O precursor. The deposition temperature was kept constant at 150 °C. The electronic properties of this TiO_2 layer are shown in more detail elsewhere.[26]

DOI: 10.1021/jp506349t
J. Phys. Chem. C 2015, 119, 2096−2104

2.4. UV−Vis Absorption and Film Thickness Measurements. The UV−vis absorption spectra of the $CuWO_4$ films were measured using a spectrometer (PerkinElmer-Lambda 900) equipped with an integrated sphere device allowing simultaneous recording of both transmittance and diffuse reflectance of the sample. Measurements were conducted for back illumination, before and after Au NP and TiO_2 layer deposition, so that the influence of each component on the overall absorption spectra could be determined.

2.5. Photoelectrochemical Measurements. The photoelectrochemical characterization of the samples, before and after their functionalization with NPs (cf. subsection 2.2 and 2.3), was carried out in an aqueous 0.1 M potassium phosphate buffer solution (KPi, K_2HPO_4, and KH_2PO_4, 99.5% Fluka, pH ∼ 7) in an electrochemical cell using a three-electrode configuration: a working electrode whose potential was controlled by a potentiostat (EG&G PAR 283), a reference Ag/AgCl electrode (XR300, saturated KCl + AgCl solution (KS120), Radiometer Analytical), and a coiled Pt wire as a counter electrode. White-light photocurrent measurements were performed under simulated AM1.5 solar illumination with a Newport Sol3A Class AAA solar simulator (type 94023A-SR3) (irradiation spectrum, Figure S1, Supporting Information). The monochromatic photocurrents (IPCE and APCE) were measured at 1.23 V vs RHE using a 200 W quartz tungsten−halogen lamp coupled into a grating monochromator with a 6 nm step following the method described in detail elsewhere.[27] IPCE measurements provide information about the number of photons incident on the photoelectrochemical cell that are effectively converted into photocurrent as a function of wavelength. This value is, however, understated due to losses associated with incident light reflection and imperfect absorption and is referred to as the external quantum efficiency.[28] The APCE is the IPCE value corrected with regard to the UV−vis absorption spectra of each sample and provides values closer to the real conversion efficiency, i.e., the internal quantum efficiency.

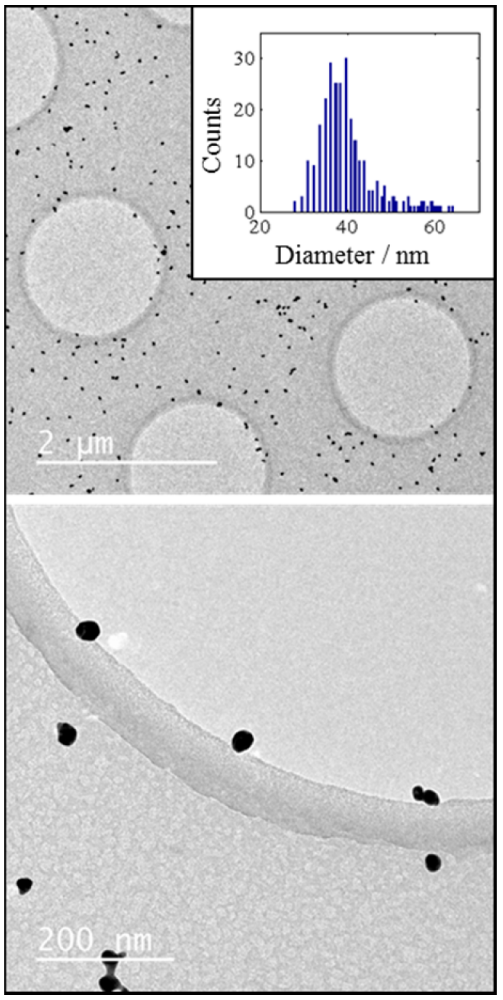

Figure 4. TEM micrographs of Au NPs produced by the spark discharge generator and selected by the DMA (as described in Figure 3). Inset figure: Size histogram of the top image.

3. RESULTS AND DISCUSSION

The size and shape of the Au NPs was measured by TEM (cf. Figure 4). The size (39 ± 7 nm) is in good agreement with that selected by the DMA (set to select 35 nm particles). The 4 nm difference between the targeted and obtained mean size can be explained by the errors involved in assuming the NPs are perfectly round. This inexact assumption (see elongated shape in Figure 4 bottom) was made in the gas-phase size selection (cf. eq S1 in the Supporting Information) and in the NP size measurements (see subsection 2.2). According to Mie theory, the λ_{max} of absorption (the wavelength where the absorption is the greatest) of an isolated 39 nm round Au particle does not deviate significantly (less than 2 nm) from the λ_{max} of the targeted 35 nm particles. Hence, we still expect that the synthesized particles, having the particle size distribution shown in the inset of Figure 4, exhibit a λ_{max} at the $CuWO_4$ band gap edge (∼540 nm).

Two configurations of $CuWO_4$−NP composites were constructed (cf. Figure 2). Configuration I (cf. Figure 2A), was fabricated by spray deposition of $CuWO_4$ on a FTO substrate, followed by Au NP deposition and TiO_2 atomic layer deposition. For Configuration II (cf. Figure 2B), first Au NPs were deposited on the FTO substrate, followed by $CuWO_4$ spray deposition on top of them. Top view SEM images of the resulting composite samples are shown in Figure 2C (Configuration I) and Figure 2D (Configuration II).

The role of the TiO_2 layer in Configuration I is 2-fold: (1) to fix the NPs on the $CuWO_4$ surface and (2) to coat the NPs in order to enhance their SPR interaction with light (Mie theory). The conduction of holes through this ultrathin insulating film is possible via tunneling.[29]

Figure 5A shows the effect of the NPs and the TiO_2 layer on the composite's (Configuration I) light absorption. The bare Au NPs increased the light absorption of $CuWO_4$ only ∼7% (at 520 nm). However, a clear red shift and increase in the peak of absorption (e.g., ∼ 12% at 544 nm) was obtained after the TiO_2 was deposited. This change is attributed to the expected effect of the SPR absorption when the NPs are coated (cf. Figure 5B). As a consequence, the coated NPs' SPR enhanced the light absorption of the $CuWO_4$ film along a larger range in the spectrum. Therefore, the SPR enhancement mechanisms (e.g., PRET) can be active over a larger range in the $CuWO_4$ thin-film absorption spectra. Moreover, the λ_{max} of absorption is located exactly at the band gap edge of $CuWO_4$ (i.e., between 540 and 550 nm). Obtaining the SPR peak of absorption in this region has two main advantages: (1) It allows us to identify the contribution, if any, of the hot electron injection mechanism since any PEC enhancement at energies beyond the $CuWO_4$

DOI: 10.1021/jp506349t
J. Phys. Chem. C 2015, 119, 2096−2104

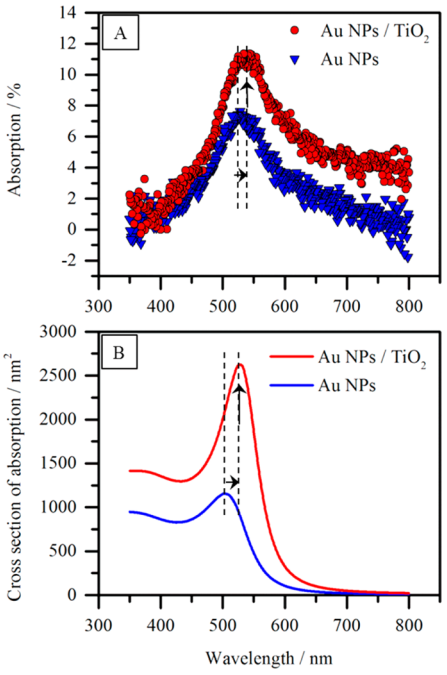

Figure 5. (A) Measured NPs' SPR absorption peak before (blue) and after (red) deposition of a TiO_2 layer of 2 nm. (B) SPR absorption cross section of coated and uncoated 39 nm NPs, according to Mie theory. The arrows indicate the red shift and the increase of the measured (top) and calculated (bottom) peak of absorption.

band gap would indicate hot electron injection from the NPs to the semiconductor (cf. subsection 1.3). On the other hand, if the enhancement is restricted to the absorption range of $CuWO_4$, despite the large NP absorption beyond the band gap edge, the hot electron mechanism can be excluded. (2) Since bare $CuWO_4$ exhibits an extremely low light absorption coefficient at these wavelengths (490−550 nm), a larger NP coverage could be used to significantly enhance the absorption in this region (through scattering or PRET mechanisms), without blocking the light at wavelengths where $CuWO_4$ efficiently absorbs light (e.g., 350 nm).

Although the λ_{max} of absorption (cf. Figure 5A) agrees with the theory (cf. Figure 5B), the width of the peak of absorption is much broader than for the isolated particle model. This can be explained by the distribution of NP sizes present on the composite (cf. Figure 4) and by the formation of dimers and larger agglomerates during the NP deposition, as shown by SEM (cf. Figure 2C). The latter also explains the absorption intensity at longer wavelengths (e.g., 700 nm) since dimers, for instance, give a second peak of absorption at longer wavelengths.[30]

The IPCE measurements for a 200 nm $CuWO_4$ film before and after functionalization with NPs (Configuration I) are shown in Figure 6A, together with their corresponding absorption spectra (Figure 6B). The absorption contribution of the TiO_2-coated Au NPs is added in Figure 6B as a reference. A significant increase in the IPCE was achieved for Configuration I. The IPCE values in Figure 6 can be used to compute the NP enhancement factor (f_{total}) as a function of the wavelength (cf. eq 1). The largest IPCE increase is observed at a wavelength of ~390 nm with an enhancement factor as large as 6-fold.

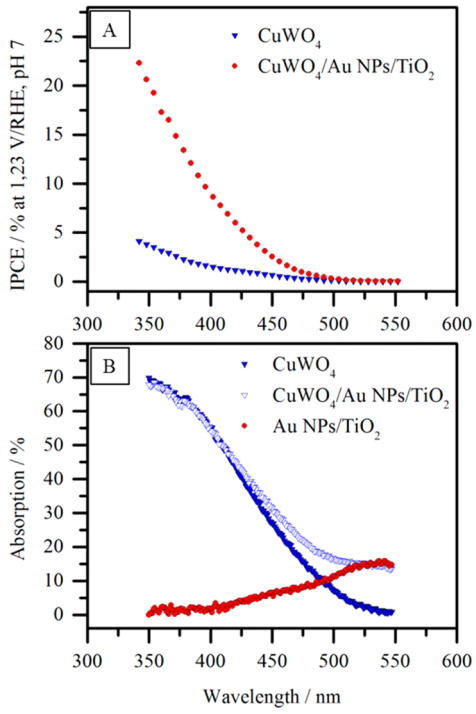

Figure 6. (A) Back illumination IPCE for the 200 nm $CuWO_4$ before and after NP functionalization (Configuration I). (B) Corresponding absorption spectra.

$$f_{total} = \frac{IPCE^{H_2O}_{CuWO_4/Au\ NPs/TiO_2}}{IPCE^{H_2O}_{CuWO_4}} \quad (1)$$

where the $IPCE^{H_2O}_{CuWO_4/Au\ NPs/TiO_2}$ and $IPCE^{H_2O}_{CuWO_4}$ are the water-splitting IPCE measurements for the composite and bare $CuWO_4$, respectively.

The enhancement of the photocurrent density ($J^{H_2O}_{photocurrent}$) of the $CuWO_4$ film is a consequence of a surface (e.g., catalytic) and/or a bulk (i.e., absorption or charge separation enhancement) effect due to the semiconductor's interaction with the decorating NPs, as stated in the following equation[31]

$$J^{H_2O}_{photocurrent} = J_{absorbed} \times P_{charge\ separation} \times P_{charge\ injection} \quad (2)$$

where $J_{absorbed}$ is the rate of photon absorption; $P_{charge\ separation}$ is the charge separation yield of photogenerated charge carriers; and $P_{charge\ injection}$ is the charge injection yield to the electrolyte.

In order to distinguish between these contributions (surface and bulk effects) we used the following strategy that was first used by Dotan et al.[31] to quantify bulk and surface recombination in Fe_2O_3 and more recently by Abdi et al.[16] to distinguish between the catalytic effect and plasmonic effect of $Ag@SiO_2$ core−shell NPs in $BiVO_4$.

By adding H_2O_2 (an easily oxidized hole scavenger) to the electrolyte, it is reasonable to assume that the surface catalytic efficiency is 100% ($P_{charge\ injection}$ = 1 in eq 2).[31] This way, the IPCE performance of bare $CuWO_4$ ($IPCE^{H_2O_2}_{CuWO_4}$) and the composite ($IPCE^{H_2O_2}_{CuWO_4/Au\ NPs/TiO_2}$) can be compared under 100% surface catalytic efficiency conditions. Any photocurrent enhancement, under these conditions ($P_{charge\ injection}$ = 1), could be then ascribed to an increase in the absorption and/or charge separation yield through a NP plasmonic effect[16]

DOI: 10.1021/jp506349t
J. Phys. Chem. C 2015, 119, 2096−2104

$$f_{\text{plasmonic}} = \frac{\text{IPCE}^{H_2O_2}_{CuWO_4/\text{Au NPs}/TiO_2}}{\text{IPCE}^{H_2O_2}_{CuWO_4}} \quad (3)$$

where $f_{\text{plasmonic}}$ is the plasmonic enhancement factor.

The catalytic enhancement ($f_{\text{catalytic}}$) can be computed by comparing the actual enhancement factor (f_{total}, cf. eq 1) and the plasmonic enhancement factor ($f_{\text{plasmonic}}$)

$$f_{\text{catalytic}} = \frac{f_{\text{total}}}{f_{\text{plasmonic}}} \quad (4)$$

Figure 7 shows the computed IPCE enhancement factors. The surface catalytic effect is found to be the predominant effect in the total enhancement, increasing the IPCE more than 3-fold at a wavelength of 390 nm. The shape of this enhancement ($f_{\text{catalytic}}$ vs wavelength) follows the light intensity spectrum used in the IPCE experiments (see Figure S2, Supporting Information), with both curves presenting a peak at ~390 nm. This can be explained by the fact that for bare $CuWO_4$, having a low catalytic efficiency, more hole surface accumulation and subsequent recombination take place when more holes are available at the surface (i.e., at wavelengths with a large incident photon flux and a corresponding higher absorption in the films). Therefore, we see that after NP functionalization the catalytic efficiency is enhanced, hindering the hole recombination to a larger extent at wavelengths (350−425 nm) with a large number of incoming photons and a relatively large $CuWO_4$ absorption coefficient.

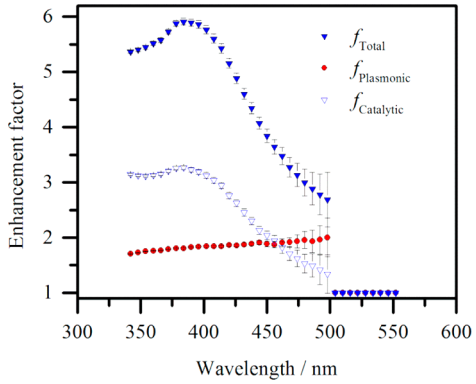

Figure 7. IPCE enhancement factors after NP functionalization (Configuration I), calculated with eqs 1, 3, and 4 from the IPCE values plotted in Figure S3 (Supporting Information). The error bars represent the sensitivity of the IPCE enhancement factors to the experimental uncertainties.

On the other hand, the curve of the calculated plasmonic enhancement factor ($f_{\text{plasmonic}}$ vs wavelength) does not increase with the intensity of the incoming light nor with the absorption of the semiconductor but with the absorption of the plasmonic NPs. Interestingly, the enhancement threshold of $f_{\text{plasmonic}}$ is limited to the wavelength range at which the bare $CuWO_4$ absorbs light. Therefore, we conclude that the hot electron injection mechanism does not play a relevant role in the measured enhancement.

In order to distinguish between the remaining plasmonic mechanisms (i.e., PRET and light scattering), the APCE enhancement factors were calculated, analogously to the IPCE enhancement factor calculations (cf. eqs 1, 3, and 4). The APCE plasmonic enhancement factor is found to be larger than 1 (cf. Figure S4, Supporting Information). An increase in the APCE, due to a plasmonic effect, cannot be explained by the scattering mechanism (assuming that the recombination properties of $CuWO_4$ are not absorption dependent) since its only contribution is to increase the absorption in the bulk of the material. The PRET mechanism, on the other hand, is characterized by a strong localized electric field (NP's near-field) that can enhance the rate of electron/hole formation of the semiconductor when the NPs are sitting on the semiconductor−electrolyte interface (near the SCL region).[18] This strong interaction between the NP's near-field and the SCL region could explain the APCE plasmonic enhancement factor shown in Figure S4 (Supporting Information). This scenario is realistic for a semiconductor whose bulk charge carrier transport is the limiting step in the PEC performance. In this case, the charge carriers formed in the bulk have a high probability for recombination, and only the electron−hole created near the surface, which undergoes efficient separation due to the SCL, contributes significantly to the total photocurrent. Hence, if this is the case for $CuWO_4$, concentrating the light intensity at the SCL with plasmonic NPs (via PRET) leads to an enhancement in the concentration of well-separated charge carriers and thus an observable APCE enhancement.

To further elucidate the effect of plasmonic NPs on the $CuWO_4$ water-splitting PEC performance, a second composite (Configuration II) was tested. For this configuration, the PRET enhancement mechanism is expected to have a much smaller effect, since the NP near-field does not concentrate the light at the electrolyte interface where the charge carriers are separated more efficiently (cf. section 1.1). Therefore, the effect of other enhancement mechanisms (e.g., scattering) that might enhance the performance to a smaller extent can be observed and studied independently.

The IPCE results of Configuration II are shown in Figure 8A, together with their corresponding absorption spectra (cf. Figure 8B). Unlike for Configuration I, for Configuration II it is not possible to measure the performance of the $CuWO_4$ film before and after NP functionalization since for this configuration (II) the NPs had to be deposited first (see Figure 2B). Therefore, Figure 8 shows the IPCE and absorption of two different samples, synthesized under exactly the same conditions, with the only difference being that the spray pyrolysis deposition of the bare $CuWO_4$ sample was made on a clean FTO surface, while the spray deposition of the composite was made on an FTO surface decorated with NPs. The maximum absorption of the bare $CuWO_4$ sample (350 nm) is 7% larger than the composite sample. This small absorption deviation comes from the thickness deviation between different spray pyrolysis depositions. The IPCE of the bare $CuWO_4$ sample and the composite (Configuration II) is almost identical (cf. Figure 8A). Nevertheless, the composite shows a small enhancement at shorter wavelengths (350−420) as shown in Figure 9. This enhancement increases with decreasing wavelength and is nonexistent at the wavelengths where the semiconductor's absorption overlaps with the NP's absorption. Therefore, we conclude that, unlike for Configuration I, Configuration II exhibits no plasmonic enhancement.

In order to explain the small increase in the performance of Configuration II, the catalytic efficiency (C_{eff}, see eq S3 in the Supporting Information) of the samples was investigated (cf. Figure S5, Supporting Information). It is observed that the composite sample has a larger catalytic efficiency, which

DOI: 10.1021/jp506349t
J. Phys. Chem. C 2015, 119, 2096−2104

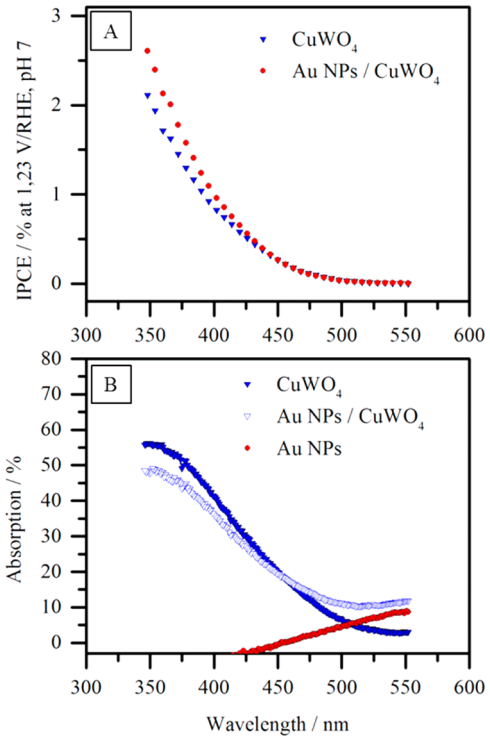

Figure 8. (A) Back illumination IPCE for bare 200 nm $CuWO_4$ and functionalized (Configuration II) 200 nm $CuWO_4$. (B) Corresponding absorption spectra.

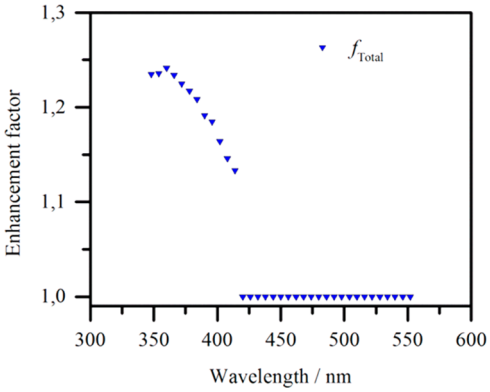

Figure 9. IPCE enhancement factor due to NP functionalization (Configuration II), calculated with eqs 1, from the IPCE values plotted in Figure 8A.

explains the small increase in the IPCE for Configuration II (cf. Figure 9). This catalytic effect can still come from the NPs, despite the fact that for Configuration II the NPs are on the back contact. This is because the $CuWO_4$ film is quite porous, and some of the NPs on the back contact can still be in contact with the electrolyte and the $CuWO_4$ grains, playing a catalytic role. This explanation is supported by SEM (Figure 2D), where some of the NPs on the FTO are still observable between the $CuWO_4$ grains.

The IPCE enhancement observed for Configuration I is found to be a contribution between a surface (NP catalytic effect) and a bulk (plasmonic effect). The plasmonic enhancement is explained here by a PRET-induced localized increase in the charge carrier yield at the SCL. This charge carrier increase at the SCL plays an important role in the $CuWO_4$'s improved photocurrent due to excellent charge separation in this region. This theory is supported by a second configuration (Configuration II) where the particles were embedded toward the back of the semiconductor, away from the SCL, and no plasmonic enhancement was observed. Furthermore, the significant plasmonic enhancement factor, obtained in this work (Figure 7), can be explained by the fact that $CuWO_4$ exhibits high bulk charge carrier recombination[5] since, in this case, any charge carrier increase at the SCL leads to a significant increase of the overall photocurrent. The PRET effect, at the SCL, has already been observed for TiO_2,[12] which also suffers from high bulk charge carrier recombination.[32]

It is important to highlight that PRET, as any plasmonic enhancement mechanism, is only active in the region of the spectrum where the NPs interact with light. In this work, the measured plasmonic enhancement factor increases with the wavelength (Figure 7), following the trend of the NP's absorption spectra. However, at shorter wavelengths (i.e., 350−400 nm) the measured NP absorption vanishes, while the enhancement factor does not decrease to unity. This enhancement in the UV region cannot be explained by a plasmonic mechanism unless even small NP absorptions (below the noise level of the used spectrometer) can have a PRET effect in the ultraviolet region of the spectrum due to the optimum absorption of the semiconductor in this region. This explanation is supported by the Mie theory calculations that show that Au NPs with a thin TiO_2 coating exhibit an absorption cross section at these wavelengths (i.e., 350−400 nm, Figure 5B). Nevertheless, other nonplasmonic contributions can also play a role in the presented enhancement, and further work must be carried out to determine them.

In addition to the plasmonic enhancement effect, an outstanding IPCE increase (3-fold at wavelengths between 350 and 410 nm) in the surface catalysis of the semiconductor was achieved for Configuration I. As shown in Figure S3 (Supporting Information), the fabricated composite exhibits nearly 100% catalytic efficiency.

The total IPCE enhancement factor for Configuration I ranged from 6- to 3-fold throughout the band gap energies of the semiconductor. This increase in the external quantum efficiency was reflected in the output photocurrent under solar simulated irradiation (see cyclic voltammetry measurements in Figure 10) with an outstanding increase of 4-fold at, for instance, 1.23 and 1.9 V vs RHE. Furthermore, in order to investigate the stability/photocorrosion properties of Configuration I, the bare and the composite samples were illuminated

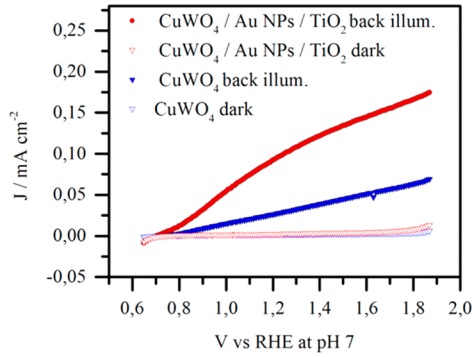

Figure 10. Three-electrode AM1.5 photocurrent versus voltage (j−v) curve of bare 200 nm $CuWO_4$ and functionalized (configuration I) 200 nm $CuWO_4$ at pH ∼7.

DOI: 10.1021/jp506349t
J. Phys. Chem. C 2015, 119, 2096−2104

with AM 1.5 irradiation under a constant applied potential (1.23 V vs RHE) while recording the current density as a function of time (cf. Figure 11). It can be observed that both

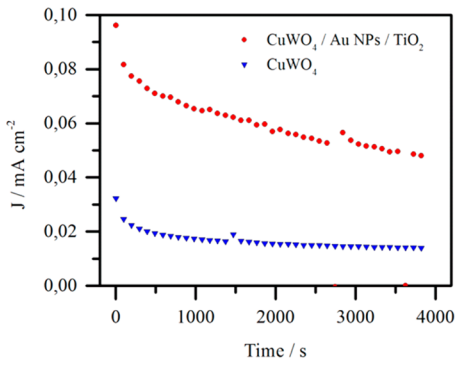

Figure 11. $j-t$ curves for $CuWO_4$ and functionalized (Configuration I) $CuWO_4$, carried out in 0.1 M KPi buffer (pH ~7) at 1.23 V vs RHE under AM 1.5 irradiation.

samples decrease their performance over time. Nevertheless, the photocurrent density of the functionalized sample is ~3 times larger than that for the bare sample for the duration of the measurement (1 h). The instability of $CuWO_4$, under the conditions used in this work, has already been shown by Yourey et al.[11] The decrease in the performance of Configuration I is found to be similar to the state of the art $CuWO_4$ films that produce similar photocurrents.[11] Therefore, we conclude that the instability of the composite sample (Configuration I) is typical of $CuWO_4$ under these conditions.

Finally, it is important to highlight that the main objective of this work was not to achieve the highest performing $CuWO_4$ but to investigate the potential plasmonic NP mechanisms that can improve the PEC performance of the material. However, we have shown that plasmonic NPs can increase significantly the photocurrent of $CuWO_4$ films. Specifically, we enhanced the photocurrent density (under simulated solar irradiation) of a 200 nm spray pyrolysis deposited $CuWO_4$ film from 0.03 to 0.1 mA·cm^{-2} (cf. Figures 10 and 11) at the thermodynamic potential for water oxidation (1.23 V vs RHE) in a pH 7 KPi solution, which is comparable to the state-of-the-art bare $CuWO_4$ film (0.15 mA·cm^{-2}), prepared by spin-casting a sol–gel-like precursor.[11] To achieve higher photocurrents, further work must be carried out to optimize the NP's coverage concentration, size, and material to achieve a higher enhancement factor.

4. CONCLUSIONS

An elegant gas-phase methodology for the synthesis and subsequent deposition of metal NPs on semiconductors has been introduced. This method was found to be an ideal way to functionalize a semiconductor surface with plasmonic NPs that interact with light in a predefined region of the spectrum. In this work, Au NPs, with a SPR λ_{max} of absorption located at the same position as the $CuWO_4$ band gap edge, were deposited on the $CuWO_4$ surface (Configuration I) or at its back contact (Configuration II).

The presented results indicate that decorating the $CuWO_4$ film surface (configuration I) with TiO_2-coated Au NPs can enhance significantly the PEC water-splitting performance of $CuWO_4$ films. The nature of this enhancement is found to be a contribution of a surface catalytic effect and a plasmonic effect.

The plasmonic contribution was quantified by comparing IPCE performance of the bare and functionalized samples under 100% surface catalytic conditions. When the particles were placed at the semiconductor–electrolyte interface (Configuration I), a plasmonic enhancement factor of ~2 was achieved. This enhancement is explained here by a PRET-induced increase in the formation of charge carriers at the SCL, where the charge carriers are separated efficiently. When NPs were placed at the back contact of the $CuWO_4$ film (Configuration II), no plasmonic enhancement was observed. This can be explained by the fact that for Configuration II, unlike Configuration I, the formation of additional charge carriers through PRET takes place at the bulk of the $CuWO_4$ film, where charge recombination is predominant.

Overall, this work is expected to have a relevant influence on future research toward improving the PEC performance of $CuWO_4$ and other semiconductors with an indirect band gap. Additionally, the method we introduced provides an easy way to distinguish the contributions of the two above-mentioned NP enhancement mechanisms (scattering and PRET), by comparing IPCE and APCE of the functionalized samples (Configurations I and II).

■ ASSOCIATED CONTENT

Supporting Information

Figures S1–S6 and equations S1–S3. This material is available free of charge via the Internet at http://pubs.acs.org.

■ AUTHOR INFORMATION

Corresponding Author

*E-mail: w.smith@tudelft.nl. Tel.: +31(0)152782659. Fax: +31(0)152787421.

Notes

The authors declare no competing financial interest.

■ ACKNOWLEDGMENTS

Financial support from the VENI project (granted to Dr. Wilson A. Smith) by NWO is gratefully acknowledged. Financial support from the NWONANO project (11521), in which the particle production method was optimized, is gratefully acknowledged. We thank Phaedra Oikonomopoulou for the illustrations, Timo van Drenth for valuable discussions, and Joost Middelkoop for the TEM measurements.

■ REFERENCES

(1) Kavan, L.; Grätzel, M.; Gilbert, S. E.; Klemenz, C.; Scheel, H. J. Electrochemical and Photoelectrochemical Investigation of Single-Crystal Anatase. *J. Am. Chem. Soc.* **1996**, *118*, 6716–6723.

(2) Kudo, A.; Miseki, Y. Heterogeneous Photocatalyst Materials for Water Splitting. *Chem. Soc. Rev.* **2009**, *38*, 253–278.

(3) Dare-Edwards, M. P.; Goodenough, J. B.; Hamnett, A.; Trevellick, P. R. Electrochemistry and Photoelectrochemistry of Iron(III) Oxide. *J. Chem. Soc., Faraday Trans. 1: Phys. Chem. Condens. Phases* **1983**, *79*, 2027–2041.

(4) Yourey, J. E.; Bartlett, B. M. Electrochemical Deposition and Photoelectrochemistry of CuWO4, a Promising Photoanode for Water Oxidation. *J. Mater. Chem.* **2011**, *21*, 7651–7660.

(5) Chang, Y.; Braun, A.; Deangelis, A.; Kaneshiro, J.; Gaillard, N. Effect of Thermal Treatment on the Crystallographic, Surface Energetics, and Photoelectrochemical Properties of Reactively Cosputtered Copper Tungstate for Water Splitting. *J. Phys. Chem. C* **2011**, *115*, 25490–25495.

(6) Varghese, O. K.; Grimes, C. A. Appropriate Strategies for Determining the Photoconversion Efficiency of Water Photo

DOI: 10.1021/jp506349t
J. Phys. Chem. C 2015, 119, 2096–2104

Electrolysis Cells: A Review with Examples Using Titania Nanotube Array Photoanodes. *Sol. Energy Mater. Sol. Cells* **2008**, *92*, 374−384.
(7) Gaillard, N.; Chang, Y.; DeAngelis, A.; Higgins, S.; Braun, A. A Nanocomposite Photoelectrode Made of 2.2 Ev Band Gap Copper Tungstate (CuWO4 and Multi-Wall Carbon Nanotubes for Solar-Assisted Water Splitting. *Int. J. Hydrogen Energy* **2013**, *38*, 3166−3176.
(8) Souza, F. L.; Lopes, K. P.; Longo, E.; Leite, E. R. The Influence of the Film Thickness of Nanostructured alpha-Fe2O3 on Water Photooxidation. *Phys. Chem. Chem. Phys.* **2009**, *11*, 1215−1219.
(9) Pandey, P. K.; Bhave, N. S.; Kharat, R. B. Spray Deposition Process of Polycrystalline Thin Films of CuWO4 and Study on Its Photovoltaic Electrochemical Properties. *Mater. Lett.* **2005**, *59*, 3149−3155.
(10) Yourey, J. E.; Kurtz, J. B.; Bartlett, B. M. Water Oxidation on a CuWO4−WO3 Composite Electrode in the Presence of [Fe(Cn)6]-3−: Toward Solar Z-Scheme Water Splitting at Zero Bias. *J. Phys. Chem. C* **2012**, *116*, 3200−3205.
(11) Yourey, J. E.; Pyper, K. J.; Kurtz, J. B.; Bartlett, B. M. Chemical Stability of CuWO4 for Photoelectrochemical Water Oxidation. *J. Phys. Chem. C* **2013**, *117*, 8708−8718.
(12) Ingram, D. B.; Linic, S. Water Splitting on Composite Plasmonic-Metal/Semiconductor Photoelectrodes: Evidence for Selective Plasmon-Induced Formation of Charge Carriers Near the Semiconductor Surface. *J. Am. Chem. Soc.* **2011**, *133*, 5202−5205.
(13) Gomes Silva, C.; Juárez, R.; Marino, T.; Molinari, R.; García, H. Influence of Excitation Wavelength (UV or Visible Light) on the Photocatalytic Activity of Titania Containing Gold Nanoparticles for the Generation of Hydrogen or Oxygen from Water. *J. Am. Chem. Soc.* **2010**, *133*, 595−602.
(14) Thimsen, E.; Le Formal, F.; Gratzel, M.; Warren, S. C. Influence of Plasmonic Au Nanoparticles on the Photoactivity of Fe2O3 Electrodes for Water Splitting. *Nano Lett.* **2010**, *11*, 35−43.
(15) Grabowska, E.; Zaleska, A.; Sorgues, S.; Kunst, M.; Etcheberry, A.; Colbeau-Justin, C.; Remita, H. Modification of Titanium(IV) Dioxide with Small Silver Nanoparticles: Application in Photocatalysis. *J. Phys. Chem. C* **2013**, *117*, 1955−1962.
(16) Abdi, F. F.; Dabirian, A.; Dam, B.; van de Krol, R. Plasmonic Enhancement of the Optical Absorption and Catalytic Efficiency of Bivo4 Photoanodes Decorated with Ag@SiO2 Core-Shell Nanoparticles. *Phys. Chem. Chem. Phys.* **2014**, *16*, 15272−15277.
(17) Warren, S. C.; Thimsen, E. Plasmonic Solar Water Splitting. *Energy Environ. Sci.* **2012**, *5*, 5133−5146.
(18) Linic, S.; Christopher, P.; Ingram, D. B. Plasmonic-Metal Nanostructures for Efficient Conversion of Solar to Chemical Energy. *Nat. Mater.* **2011**, *10*, 911−921.
(19) Kelly, K. L.; Coronado, E.; Zhao, L. L.; Schatz, G. C. The Optical Properties of Metal Nanoparticles: The Influence of Size, Shape, and Dielectric Environment. *J. Phys. Chem. B* **2002**, *107*, 668−677.
(20) Derkacs, D.; Lim, S. H.; Matheu, P.; Mar, W.; Yu, E. T. Improved Performance of Amorphous Silicon Solar Cells Via Scattering from Surface Plasmon Polaritons in Nearby Metallic Nanoparticles. *Appl. Phys. Lett.* **2006**, *89*, 093103.
(21) Kamat, P. V. Photophysical, Photochemical and Photocatalytic Aspects of Metal Nanoparticles. *J. Phys. Chem. B* **2002**, *106*, 7729−7744.
(22) Schwyn, S.; Garwin, E.; Schmidt-Ott, A. Aerosol Generation by Spark Discharge. *J. Aerosol Sci.* **1988**, *19*, 639−642.
(23) Hinds, W. C. Chapter 15 Electrical Properties. In *Aerosol Technology: Properties, Behavior, and Measurement of Airborne Particles*; John Wiley: New York, 1999; pp 316−347.
(24) Knutson, E. O.; Whitby, K. T. Aerosol Classification by Electric Mobility: Apparatus, Theory, and Applications. *J. Aerosol Sci.* **1975**, *6*, 443−451.
(25) Ritala, M.; Niinisto, J., Chapter 4 Atomic Layer Deposition. In *Chemical Vapour Deposition: Precursors*; The Royal Society of Chemistry: 2009; pp 158−206.
(26) Digdaya, I.; Han, L.; Buijs, T.; Zeman, M.; Dam, B.; Smets, A. H. M.; Smith, W. A. Improved photovoltage and performance of a-SiC photocathodes by the addition of a TiO2 front surface field layer. *Energy Environ. Sci.* **2014**, submitted.
(27) Abdi, F. F.; van de Krol, R. Nature and Light Dependence of Bulk Recombination in Co-Pi-Catalyzed BiVO4 Photoanodes. *J. Phys. Chem. C* **2012**, *116*, 9398−9404.
(28) Murphy, A. B.; Barnes, P. R. F.; Randeniya, L. K.; Plumb, I. C.; Grey, I. E.; Horne, M. D.; Glasscock, J. A. Efficiency of Solar Water Splitting Using Semiconductor Electrodes. *Int. J. Hydrogen Energy* **2006**, *31*, 1999−2017.
(29) Hu, S.; Shaner, M. R.; Beardslee, J. A.; Lichterman, M.; Brunschwig, B. S.; Lewis, N. S. Amorphous TiO2 Coatings Stabilize Si, GaAs, and GaP Photoanodes for Efficient Water Oxidation. *Science* **2014**, *344*, 1005−1009.
(30) Kadkhodazadeh, S.; de Lasson, J. R.; Beleggia, M.; Kneipp, H.; Wagner, J. B.; Kneipp, K. Scaling of the Surface Plasmon Resonance in Gold and Silver Dimers Probed by Eels. *J. Phys. Chem. C* **2014**, *118*, 5478−5485.
(31) Dotan, H.; Sivula, K.; Gratzel, M.; Rothschild, A.; Warren, S. C. Probing the Photoelectrochemical Properties of Hematite (alpha-Fe2O3) Electrodes Using Hydrogen Peroxide as a Hole Scavenger. *Energy Environ. Sci.* **2011**, *4*, 958−964.
(32) Yates, J. T., Jr. Photochemistry on TiO2: Mechanisms Behind the Surface Chemistry. *Surf. Sci.* **2009**, *603*, 1605−1612.

DOI: 10.1021/jp506349t
J. Phys. Chem. C 2015, 119, 2096−2104